Hydrogen Evolution Reaction

DOI: 10.1002/ange.201410050

High Catalytic Activity of Nitrogen and Sulfur Co-Doped Nanoporous Graphene in the Hydrogen Evolution Reaction**

*Yoshikazu Ito, Weitao Cong, Takeshi Fujita, Zheng Tang, and Mingwei Chen**

Abstract: *Chemical doping has been demonstrated to be an effective way to realize new functions of graphene as metal-free catalyst in energy-related electrochemical reactions. Although efficient catalysis for the oxygen reduction reaction (ORR) has been achieved with doped graphene, its performance in the hydrogen evolution reaction (HER) is rather poor. In this study we report that nitrogen and sulfur co-doping leads to high catalytic activity of nanoporous graphene in HER at low operating potential, comparable to the best Pt-free HER catalyst, 2D MoS_2. The interplay between the chemical dopants and geometric lattice defects of the nanoporous graphene plays the fundamental role in the superior HER catalysis.*

Graphene with its large surface area, high mechanical strength, and excellent electrical conductivity is an ideal electrode material for electrochemical reactions.[1] The high chemical stability of graphene ensures stable electrode performance and long electrode lifetimes but, on the other hand, implies little catalytic activity in electrochemical reactions, such as oxygen reduction reaction (ORR), oxygen evolution reaction (OER), and hydrogen evolution reaction (HER). To reduce the electrode overpotentials of these reactions, additional electrocatalysts are required thus forming graphene-based composites. For example, carbon-based metal-free composites such as carbon nitride-loaded graphene offer excellent catalytic performance for ORR,[2] OER,[3] and HER.[4] However, graphene-based composite electrodes often suffer from poor stability and low mass activity because of the weak bonding of the catalysts with graphene, the high mass density of the loaded noble metal and oxide catalysts, and the ineffective packing of 2D graphene sheets.[5] Atomic doping has been known as a feasible way to realize new functions of materials. It has been demonstrated that nitrogen-doped graphene,[6] sulfur-doped graphene,[7] and graphene oxide/reduced graphene oxide[7a,8] are active catalysts for ORR. Moreover, co-doping of graphene with nitrogen and oxygen or sulfur gives rise to synergistic effects in ORR catalysis. Although chemically doped graphene materials have shown excellent ORR catalytic activity, their HER and OER catalysis is rather poor.[9] Recently, boron/nitrogen,[10] nitrogen/sulfur,[11] and nitrogen/phosphine[9a] co-doped graphene and graphitic carbon materials have shown improved catalytic activity for OER and HER. However, the overall catalytic activity is still much lower in comparison with other Pt-free catalysts. Especially, the HER catalysis of chemically doped graphene is much lower than that of two dimensional (2D) transition metal dichalcogenides (MoS_2, WS_2, ReS_2).[12]

Here we report nitrogen and sulfur co-doped nanoporous graphene which was synthesized by nanoporous Ni-based chemical vapor deposition. The coupling between chemical dopants and the geometric lattice defects in 3D nanoporous graphene offers excellent catalytic activities towards HER, which is comparable to that of 2D MoS_2 nanosheets, the best Pt-free HER catalyst known so far.

Chemically doped nanoporous graphene was grown by chemical vapor deposition using nanoporous Ni (np-Ni)[13] as both template and substrate, and pyridine and thiophene as carbon, nitrogen and sulfur sources, respectively (Figure 1 a). np-Ni displays a three-dimensional (3D) open porosity and catalytically active internal Ni surface, resulting in the uniform growth of the chemically doped graphene on the nano-sized Ni ligament surface. Chemically doped nanoporous graphene samples were uniformly exfoliated by etching away the nanoporous Ni substrates in hydrochloric acid solution. The 3D nanoporous graphene displays bicontinuous nanopores and a high density of defective graphene structures which are geometrically required to compensate the curvature and curvature gradients, as illustrated in Figure 1 b,c. Nitrogen and sulfur co-doped graphene deposited at 800 °C (abbreviated as NS-800) for 5 min and solely sulfur (S) doped graphene deposited at 800 °C (abbreviated as S-800) for 5 min show 100–300 nm pore size (Figure S1 a,b in the Supporting Information) while NS-doped graphene deposited at 500 °C (abbreviated as NS-500) for 5 min and solely S-doped graphene deposited at 500 °C (abbreviated as S-500) for 5 min have a smaller pore size of ca. 100 nm (Figure S1 c,d). For comparison, nanoporous graphene with and without nitrogen doping was also prepared by CVD

[*] Dr. Y. Ito, W. Cong, Dr. T. Fujita, Prof. M. W. Chen
WPI Advanced Institute for Materials Research, Tohoku University
Sendai 980-8577 (Japan)
E-mail: mwchen@wpi-aimr.tohoku.ac.jp
Homepage: http://www.wpi-aimr.tohoku.ac.jp/chen_labo/
W. Cong, Prof. Z. Tang
Key Laboratory of Polar Materials and Devices, Ministry of Education of China, East China Normal University
Shanghai 200241 (China)
Prof. M. W. Chen
CREST (Japan) Science and Technology Agency
Saitama 332-0012 (Japan)

[**] This work was supported by JST-CREST ("Phase Interface Science for Highly Efficient Energy Utilization"), the fusion research funds of the World Premier International (WPI) Research Center Initiative for Atoms, Molecules and Materials, and MEXT (Japan). Z.T. was supported by the National Science Foundation of China. We thank the Institute for Material Research in Tohoku University for XPS measurements.

Supporting information for this article is available on the WWW under http://dx.doi.org/10.1002/anie.201410050.

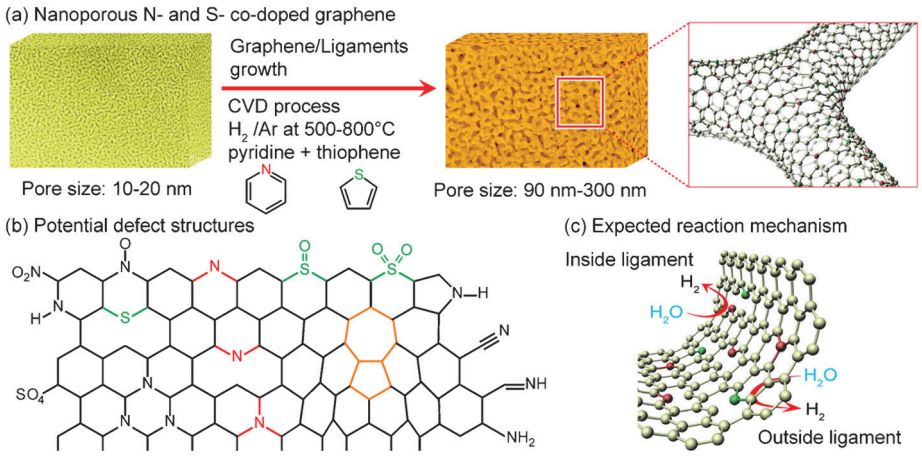

Figure 1. Illustration of the preparation process of N and S co-doped nanoporous graphene. a) Preparation of nanoporous NS-doped graphene by CVD. b) Potential defect structures in NS-doped nanoporous graphene. c) Expected reaction mechanism on nanoporous graphene.

growth at 800 °C and 500 °C using benzene or pyridine (abbreviated as G-800, G-500, N-800, and N-500) as carbon and nitrogen sources, respectively.[14] The specific surface areas and pore sizes of the nanoporous graphene samples were measured by the Brunauer–Emmett–Teller (BET)[15] and Barrett–Joyner–Hallender (BJH)[16] methods, respectively. The chemically doped nanoporous graphene samples have surface areas of 762 $m^2 g^{-1}$ and average pore size of 230 nm for NS-800, 828 $m^2 g^{-1}$ and 260 nm for S-800, 1320 $m^2 g^{-1}$ and 90 nm for NS-500, and 945 $m^2 g^{-1}$ and 90 nm for S-500 (Figure S2). Raman spectra of the chemically doped graphene show an intense D band (Figure S3 and Table S1) as compared with pristine nanoporous graphene (G-800), suggesting that the chemical doping introduces additional structure defects into the graphene lattice. According to the intensity ratio of 2D and G bands, the chemically doped graphene in the 3D nanoporous structure is mainly few-layer graphene. The average thickness of the graphene sheets in the nanoporous samples was further estimated based on their densities and BET surface areas by using 1–2 layer nanoporous pure graphene as reference. For example, the densities of NS-800 and G-800 are 5.9×10^{-4} g cm^{-3} and 3.1×10^{-4} g cm^{-3}, respectively. As G-800 consists of 1–2 layer graphene, as determined by Raman spectra (I_{2D}/I_G: 2.8), it is concluded that the graphene layer in NS-800 is 3–5. Moreover, the samples grown at 500 °C show a defective graphitic structure, together with a very weak 2D band (I_{2D}/I_G: 0.2–0.4). Thus, a lower CVD temperature leads to high intensity of D bands and broad peak width of G bands. Importantly, the at 800 °C CVD-grown samples preserve the high crystallinity of the graphene structures (I_{2D}/I_G: 0.6–0.9) without detectable amorphous carbon features (I_D/I_G: 0.5–0.8).

The microstructure of the chemically doped graphene was characterized with a Cs-corrected transmission electron microscope (TEM). Figure 2a shows a low-magnification TEM micrograph of NS-800 displaying a tubular-like graphene sheet which preserves the bicontinuous nanoporosity of the np-Ni substrate. Figure 2b shows the high-resolution TEM image (HRTEM) and the corresponding selected area electron diffraction pattern of the chemically doped graphene. The sharp diffraction spots and visible crystal lattices verify that the chemically doped graphene has high crystallinity, in accordance to the Raman spectra. The HRTEM micrograph (inset of Figure 2b) also reveals the structure defects of the graphene lattice, which appear to be related to the sites occupied by doped nitrogen and sulfur atoms (red circle). The electron energy-loss spectroscopy (EELS) mappings (Figure 2c) show that nitrogen and sulfur atoms are homogenously disperse in the nanoporous graphene. Importantly, the distribution of

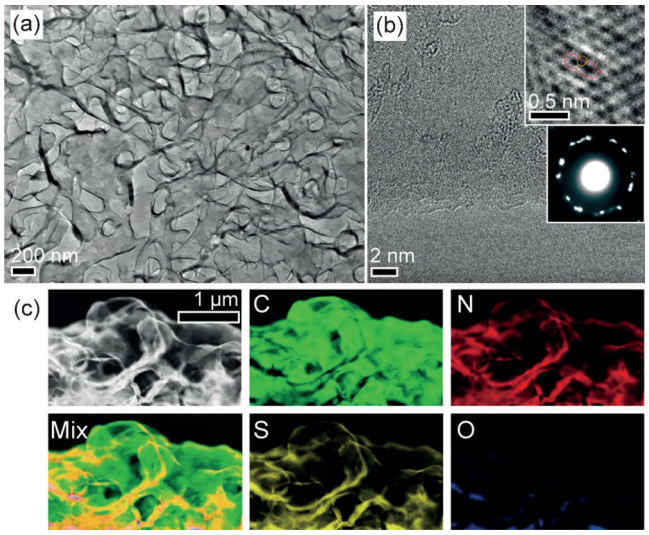

Figure 2. TEM images of NS-doped nanoporous graphene. a) Low-magnification TEM image. b) High-resolution TEM image and corresponding selected area electron diffraction pattern (lower right inset). The upper right inset highlights a defect structure of potential pyridinic nitrogen or sulfur sites. c) EELS chemical mappings of C, N, S, and O in NS-800.

nitrogen is fully coupled with that of sulfur. Oxygen can also be detected in some regions. The NS-500 sample has a very similar microstructure to NS-800, which is shown in Figure S4.

The binding state and quantitative chemical composition of the chemically doped nanoporous graphene were investigated by X-ray photoelectron spectroscopy (XPS) (Figure 3 and Figure S5). The samples grown at high temperatures show a low atomic doping level while the low-temperature CVD leads to a high concentration of dopants. For the nitrogen and sulfur co-doped graphene, various kinds of nitrogen and sulfur binding states co-exist. The N 1s XPS spectra demonstrate the formation of graphitic, pyridinic, and oxide nitrogen

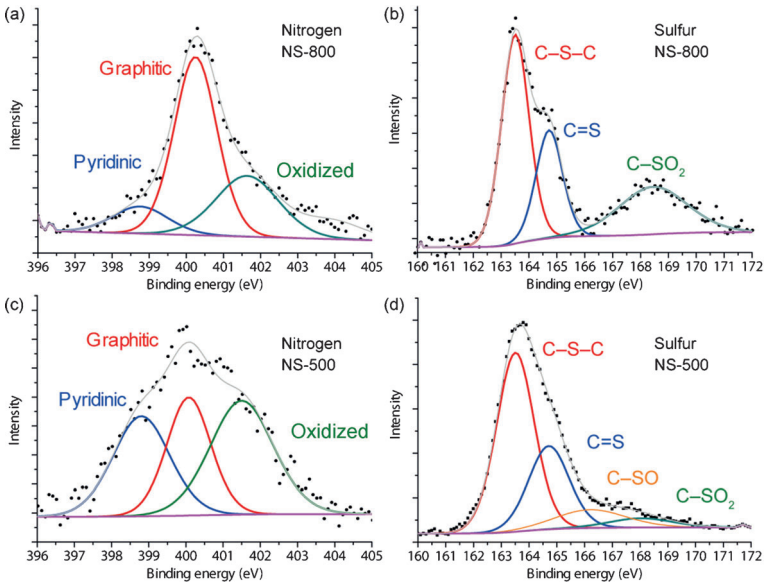

Figure 3. Chemical binding state of nanoporous NS-doped graphene. N 1s (a,c) and S 2p XPS (b,d) spectra of NS-800 (a,b) and NS-500 (c,d).

structures.[17] Moreover, the S 2p XPS spectra reveal that the binding states of sulfur are -C-S-C- (163.8 eV),[11] -C=S- (165.0 eV)[11] and -C-SO- (164.1 eV),[11,18] -C-SO_2- (168.6 eV).[11,19] The quantitative measurements are summarized in Table 1. The CVD temperature clearly influences both nitrogen and sulfur concentrations and their chemical binding states. Lower CVD temperatures give rise to higher N and S concentrations and more defective graphene structures (Figure S3). The residual Ni from the nanoporous Ni templates in the graphene samples was confirmed to be less than 0.07 at.%, and HER-active NiS could not be detected in the XPS spectra of the S-doped samples (Figure S6).

The HER catalytic performances of the nanoporous graphene samples were investigated by cyclic voltammetry (CV). Figure 4a shows the HER polarization curves in a 0.5 M H_2SO_4 aqueous solution. From the series of 800 °C CVD-grown samples, it can be seen that chemical doping significantly enhanced the HER activity of graphene as indicated by a gradual decrease in the onset potentials from G800, N800, S800, to NS800. The operating potentials at 10 mA cm^{-2} current are measured to be −0.56 V for N800, −0.48 V for S800, and −0.39 V for NS800 (Table S2). Compared with undoped and single N- or S-doped samples, the N and S co-doping drastically improves the HER catalysis of graphene. The chemical effect on the catalytic activity of graphene is further confirmed by Tafel plots (Figure 4b) and, again, the co-doped NS-800 shows the lowest Tafel slope of 105 mV/dec among the 800 °C CVD-grown samples. Apart from the direct chemical doping effect, the CVD temperatures also notably influence the catalytic activity of chemically doped graphene because low CVD temperatures can introduce more dopants and structure defects into the graphene lattice and hence change its chemical activity.[14b,17b] As shown in Figure 4a,b, N-500 and S-500 have much better catalytic activity than N-800 and S-800 with regard to onset potential and Tafel slope. However, comparing the HER activities of G-800 and G-500, it can be seen that G-500 with its carbon-defective structure does not show much improved activity, which indicates that carbon defects alone do not provide catalytic activity for HER. In contrast, NS-500 with a high density of both dopants and structural defects (Table 1) shows the best HER activities with an onset potential of −0.13 V, Tafel slope of 80.5 mV/dec and operating potential of −0.28 V at 10 mA cm^{-2}. These values are comparable to the best dichalcogenide monolayer catalysts[12a,b,20] and even better than recently developed nanoporous graphite–C_3N_4 composites and sulfur doped porous carbon materials (Table S2). Therefore, NS-500 is one of best metal-free catalysts in HER known to date. The outstanding catalytic properties of the nitrogen and sulfur co-doped graphene grown at low temperature also demonstrate that the catalytically active sites in doped graphenes are most likely associated with dopant atoms around defects, such as -C-S-C- and -C=S- structures. This assumption is supported by the fact that 4–6 at.% of the -C-S-C- and -C=S- bindings were converted to -C-SO_2- after 1000 HER cycles (Figure S7), indicating that the -C-S-C- and -C=S- are directly involved in the electrode redox reactions and responsible for the degeneration of HER catalysis during cycling. Moreover, the amount of -C-S-C- and -C=S- motifs etc. in NS-800 (0.56%) is less than in S-800 (0.90%) (Table 1). However, the former shows a higher catalytic activity. Thus, the concentration of sulfur dopant may not be the sole factor for high HER activity. The co-doped NS-800 sample contains 0.28% pyridinic nitrogen dopants. The coupling of these N dopants with the S dopants appears to play an essential role in the high HER activity of the co-doped graphene.

Table 1: Quantitative XPS measurements of chemically doped nanoporous graphene at CVD temperatures of 500 °C and 800 °C.[a]

	Graphitic C (at%)	Graphitic N (at%)	Pyridinic N (at%)	Oxidized N (at%)	-C-S-C- (at%)	-C=S- (at%)	-C-SO- (at%)	-C-SO_2- (at%)
NS-500	91.14	1.08	1.19	1.52	2.86	1.42	0.54	0.24
NS-800	96.89	1.60	0.28	0.67	0.21	0.10	–	0.25
S-500	90.69	–	–	–	4.63	2.32	0.31	2.05
S-800	99.0	–	–	–	0.51	0.26	–	0.13
N-500	93.3	4.1	1.6	1.0	–	–	–	–
N-800	97.0	1.88	0.58	0.84	–	–	–	–

[a] The carbon atom concentration was determined through the intensity of graphitic carbon.

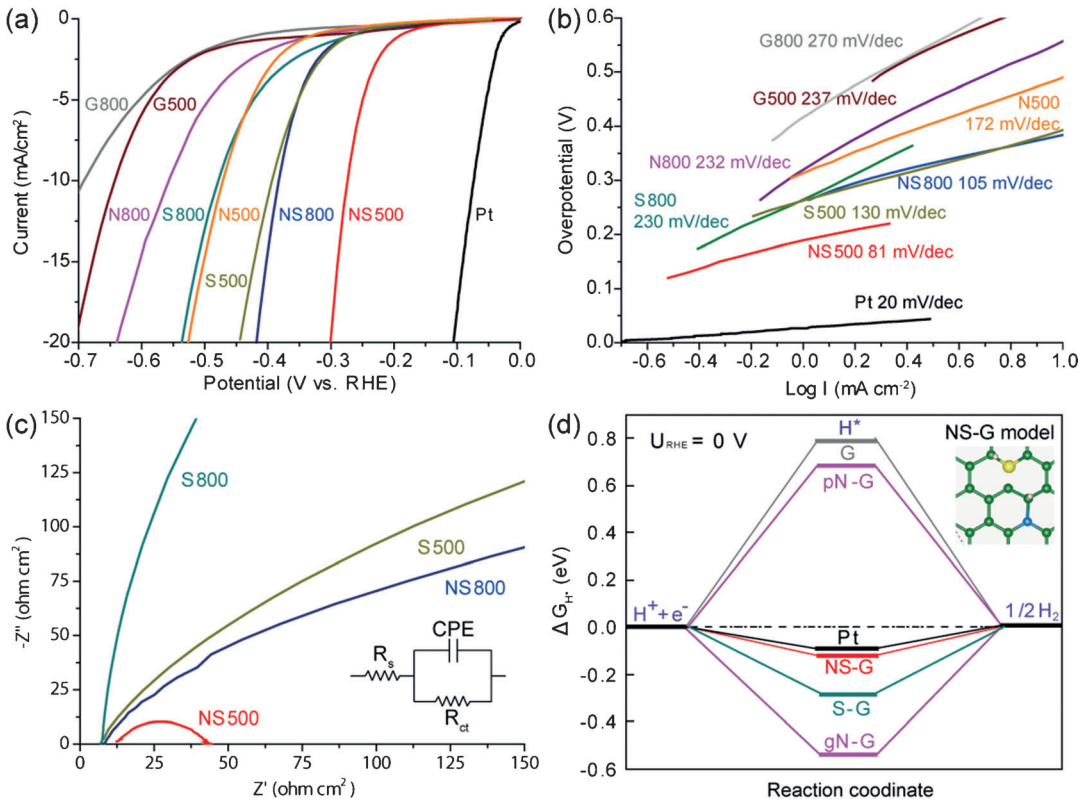

Figure 4. HER activity of chemically doped nanoporous graphenes. a) CV curves of the samples produced at different CVD temperatures and with different dopants in comparison to undoped nanoporous graphene. b) Tafel plots for the different graphene samples. c) Electrochemical impedance spectroscopy of the graphene samples at HER overpotential of −0.20 V. d) DFT-calculated HER activities of chemically doped nanoporous graphenes with a geometric lattice defect. Shown is the calculated HER free energy diagram at equilibrium potential for a Pt catalyst and for pyridinic (pN-G), graphitic (gN-G), sulfur doped (S-G), and nitrogen/sulfur co-doped (NS-G) graphene samples. The inset shows a NS-doped graphene model with a nitrogen (blue), sulfur (yellow), and hydrogen atom (white).

Electrochemical impedance spectroscopy results (Figure 4c) display lower charge-transfer resistance (R_{ct}) and internal resistance (R_s) of single- and co-doped graphene samples. Apparently, the enhanced HER performance of chemically doped graphene is related to the lower resistance of the graphene and graphene–electrolyte interface. For examples, the internal and charge-transfer resistances of NS-500 are as low as 20 $\Omega\,cm^{-2}$ and 3.6 Ω, respectively. The high electric conductivity originates from the unique bicontinuous porous structure and the high crystallinity of the chemically doped graphene as well as increased Fermi energy by chemical doping,[21] which will be detailed later. The lower charge transfer resistance of NS-500 can be attributed to the large and conductive specific surface and enhanced H^+ absorption due to the chemical doping. NS-800 and NS-500 also show high cycling stability. Electrode currents at −0.20 V were retained for ca. 90% and 60%, respectively, after 1000 cycles (Figure S8a). At a constant operating voltage of −0.20 V NS-800 kept ca. 90% durability after more than 7 days (Figure S8b). Raman spectra show that the graphene samples were still high crystallinity with slightly increased D band intensity after 1000 cycles (Figure S9). The low stability of NS-500 is most likely caused by the excess structural defects in the graphene lattice, which are not stable during the electrode reactions. Thus, removing or stabilizing unstable lattice defects and, at the same time, keeping high concentrations of S and N dopants are expected to be a viable approach to improve the electrochemical stability of NS-500.

To understand the underlying mechanisms of the co-doping enhanced HER catalysis, we performed density functional theory (DFT) calculations to investigate the electronic structure and H* absorption free energy of the NS-doped graphene. A simple structural model of a graphene lattice with one sulfur and one nitrogen atom demonstrates the existence of positively and negatively charged electron density distribution (non-electron-neutral states), which could be helpful for hydrogen generation. In addition, the Fermi level of NS-doped graphene is negatively shifted to 0.6 eV above the Dirac point (Figure S10) due to the electron-rich character of the defective structures, which could contribute to high electrical conductivity[14] and promote HER performance. The overall HER mechanism was reported with a three-state diagram consisting of 1) an initial stage of $H^+ + e^-$, 2) an intermediate stage of H* absorption, and 3) a final stage of $1/2\,H_2$ generation.[22] It is well-known that highly efficient catalysts have a Gibbs free energy of H* absorption $|\Delta G_{H^*}|$ close to zero.[22c] For example in Figure 4d, $|\Delta G_{H^*}|$ of pure graphene is positive and H* cannot efficiently absorb on the catalyst. In the case of N- or S-doped graphene, $|\Delta G_{H^*}|$ is negative and H* cannot effectively desorb from the

catalyst. Among various N- and/or S-doped graphene structures, NS-doped graphene with one carbon defect near S doping site (-C-S-C- or -C=S-) in the vicinity of graphitic N (inset of Figure 4d and Figure S11) has the smallest $|\Delta G_{H^*}|$ value of 0.12 eV, which is comparable to Pt catalyst ($|\Delta G^{Pt}_{H^*}| \approx 0.09$ eV). This local atomic configuration predicted by DFT for high efficiency hydrogen production is consistent with the XPS measurements (Figure 3 and Figure S5). The combination of the positively charged N dopants and the negatively charged S dopants at a lattice defect provides a fast electron transfer path for HER. Therefore, interplay of N and S dopants with geometric lattice defects of the nanoporous graphene plays the fundamental role in the superior HER catalysis.

In summary we have successfully synthesized nitrogen and sulfur co-doped 3D nanoporous graphene by using a nanoporous-metal-based CVD method. It was found that carbon defects alone in the graphene lattice are not catalytically active for HER while the coupling of S and N dopants with geometric defects in the graphene lattice produces an synergistic effect in tuning the Gibbs free energy of H* absorption and hence is responsible for the outstanding HER catalysis. The catalytic activity of the S and N co-doped nanoporous graphene with both high concentrations of dopants and geometric defects is comparable to MoS_2 nanosheets, the best Pt-free HER catalysts known in the literature.

Received: October 13, 2014
Revised: October 23, 2014
Published online: December 2, 2014

Keywords: chemical vapor deposition · graphene · hydrogen evolution reaction · N/S co-doping

[1] a) A. K. Geim, K. S. Novoselov, *Nat. Mater.* **2007**, *6*, 183 – 191; b) Y. Zhu, S. Murali, W. Cai, X. Li, J. W. Suk, J. R. Potts, R. S. Ruoff, *Adv. Mater.* **2010**, *22*, 3906 – 3924; c) A. Ambrosi, C. K. Chua, A. Bonanni, M. Pumera, *Chem. Rev.* **2014**, *114*, 7150 – 7188; d) D. Chen, L. Tang, J. Li, *Chem. Soc. Rev.* **2010**, *39*, 3157 – 3180; e) D. A. C. Brownson, D. K. Kampouris, C. E. Banks, *Chem. Soc. Rev.* **2012**, *41*, 6944 – 6976; f) Y. Shao, J. Wang, H. Wu, J. Liu, I. A. Aksay, Y. Lin, *Electroanalysis* **2010**, *22*, 1027 – 1036; g) J. Wu, W. Pisula, K. Müllen, *Chem. Rev.* **2007**, *107*, 718 – 747; h) Y. Zheng, Y. Jiao, M. Jaroniec, Y. Jin, S. Z. Qiao, *Small* **2012**, *8*, 3550 – 3566; i) Y. Zheng, J. Liu, J. Liang, M. Jaroniec, S. Z. Qiao, *Energy Environ. Sci.* **2012**, *5*, 6717 – 6731.

[2] a) Y. Zheng, Y. Jiao, J. Chen, J. Liu, J. Liang, A. Du, W. Zhang, Z. Zhu, S. C. Smith, M. Jaroniec, G. Q. Lu, S. Z. Qiao, *J. Am. Chem. Soc.* **2011**, *133*, 20116 – 20119; b) J. Liang, Y. Zheng, J. Chen, J. Liu, D. H. Jurcakova, M. Jaroniec, S. Z. Qiao, *Angew. Chem.* **2012**, *124*, 3958 – 3962; c) J. Liang, X. Du, C. Gibson, X. W. Du, S. Z. Qiao, *Adv. Mater.* **2013**, *25*, 6226 – 6231; d) J. Liang, Y. Zheng, J. Chen, J. Liu, D. H. Jurcakova, M. Jaroniec, S. Z. Qiao, *Angew. Chem. Int. Ed.* **2012**, *51*, 3892 – 3896; *Angew. Chem.* **2012**, *124*, 3958 – 3962; e) Z. Lin, G. H. Waller, Y. Liu, M. Liu, C.-p. Wong, *Nano Energy* **2013**, *2*, 241 – 248; f) Y. Tang, B. L. Allen, D. R. Kauffman, A. Star, *J. Am. Chem. Soc.* **2009**, *131*, 13200 – 13201; g) X. Wang, J. Wang, D. Wang, S. Dou, Z. Ma, J. Wu, L. Tao, A. Shen, C. Ouyang, Q. Liua, S. Wang, *Chem. Commun.* **2014**, *50*, 4839 – 4842; h) Y. Su, Y. Zhang, X. Zhuang, S. Li, D. Wu, F. Zhang, X. Feng, *Carbon* **2013**, *62*, 296 – 301.

[3] a) J. Tian, Q. Liu, A. M. Asiri, K. A. Alamry, X. Sun, *ChemSusChem* **2014**, *7*, 2125 – 2130; b) T. Y. Ma, J. R. Ran, S. Dai, M. Jaroniec, S. Z. Qiao, *Angew. Chem. Int. Ed.* **2014**, *53*, 7281 – 7285; *Angew. Chem.* **2014**, *126*, 7409 – 7413; c) S. Chen, J. Duan, M. Jaroniec, S. Z. Qiao, *Adv. Mater.* **2014**, *26*, 2925 – 2930.

[4] a) Y. Zheng, Y. Jiao, Y. Zhu, L. H. Li, Y. Han, Y. Chen, A. Du, M. Jaroniec, S. Z. Qiao, *Nat. Commun.* **2014**, *5*, 3783; b) W. Cui, Q. Liu, N. Cheng, A. M. Asiricd, X. Sun, *Chem. Commun.* **2014**, *50*, 9340 – 9342; c) B. Zhang, Z. Wen, S. Ci, J. Chen, Z. He, *RSC Adv.* **2014**, *4*, 49161 – 49164.

[5] a) Y. Sun, C. Li, Y. Xu, H. Bai, Z. Yao, G. Shi, *Chem. Commun.* **2010**, *46*, 4740 – 4742; b) R.-S. Zhong, Y.-H. Qin, D.-F. Niu, J.-W. Tian, X.-S. Zhang, X.-G. Zhou, S.-G. Sun, W.-K. Yuan, *J. Power Sources* **2013**, *225*, 192 – 199; Q. Liu, J. Zhang, *Langmuir* **2013**, *29*, 3821 – 3828; c) J. Jin, X. Fu, Q. Liu, J. Zhang, *J. Mater. Chem. A* **2013**, *1*, 10538 – 10545.

[6] a) S. Yang, X. Feng, X. Wang, K. Müllen, *Angew. Chem. Int. Ed.* **2011**, *50*, 5339 – 5343; *Angew. Chem.* **2011**, *123*, 5451 – 5455; b) Z. Lin, G. H. Waller, Y. Liu, M. Liu, C.-P. Wong, *Carbon* **2013**, *53*, 130 – 136; c) C. Zhang, L. Fu, N. Liu, M. Liu, Y. Wang, Z. Liu, *Adv. Mater.* **2011**, *23*, 1020 – 1024; d) W. Ding, Z. Wei, S. Chen, X. Qi, T. Yang, J. Hu, D. Wang, L.-J. Wan, S. F. Alvi, L. Li, *Angew. Chem. Int. Ed.* **2013**, *52*, 11755 – 11759; *Angew. Chem.* **2013**, *125*, 11971 – 11975; e) L. Lai, J. R. Potts, D. Zhan, L. Wang, C. K. Poh, C. Tang, H. Gong, Z. Shen, J. Lin, R. S. Ruoff, *Energy Environ. Sci.* **2012**, *5*, 7936 – 7942; f) D. Geng, Y. Chen, Y. Chen, Y. Li, R. Li, X. Sun, S. Yeb, S. Knights, *Energy Environ. Sci.* **2011**, *4*, 760 – 764; g) L. Qu, Y. Liu, J.-B. Baek, L. Dai, *ACS Nano* **2010**, *4*, 1321 – 1326; h) H. Kim, K. Lee, S. I. Woo, Y. Jung, *Phys. Chem. Chem. Phys.* **2011**, *13*, 17505 – 17510.

[7] a) Y. Jiao, Y. Zheng, M. Jaroniec, S. Z. Qiao, *J. Am. Chem. Soc.* **2014**, *136*, 4394 – 4403; b) S. Yang, L. Zhi, K. Tang, X. Feng, J. Maier, K. Müllen, *Adv. Funct. Mater.* **2012**, *22*, 3634 – 3640.

[8] Z.-H. Sheng, L. Shao, J.-J. Chen, W.-J. Bao, F.-B. Wang, X.-H. Xia, *ACS Nano* **2011**, *5*, 4350 – 4358.

[9] a) Y. Zheng, Y. Jiao, L. H. Li, T. Xing, Y. Chen, M. Jaroniec, S. Z. Qiao, *ACS Nano* **2014**, *8*, 5290 – 5296; b) L. Wang, F. Yin, C. Yao, *Int. J. Hydrogen Energy* **2014**, *39*, 15913 – 15919.

[10] a) Y. Zheng, Y. Jiao, L. Ge, M. Jaroniec, S. Z. Qiao, *Angew. Chem. Int. Ed.* **2013**, *52*, 3110 – 3116; *Angew. Chem.* **2013**, *125*, 3192 – 3198; b) S. Wang, E. Iyyamperumal, A. Roy, Y. Xue, D. Yu, L. Dai, *Angew. Chem. Int. Ed.* **2011**, *50*, 11756 – 11760; *Angew. Chem.* **2011**, *123*, 11960 – 11964.

[11] a) J. Liang, Y. Jiao, M. Jaroniec, S.-Z. Qiao, *Angew. Chem. Int. Ed.* **2012**, *51*, 11496 – 11500; *Angew. Chem.* **2012**, *124*, 11664 – 11668; b) Y. Zhang, M. Chu, L. Yang, W. Deng, Y. Tan, M. Ma, Q. Xie, *Chem. Commun.* **2014**, *50*, 6382; c) Y. Li, H. Zhang, Y. Wang, P. Liu, H. Yang, X. Yao, D. Wang, Z. Tanga, H. Zhao, *Energy Environ. Sci.* **2014**, *7*, 3720 – 3726.

[12] a) D. Voiry, M. Salehi, R. Silva, T. Fujita, M. W. Chen, T. Asefa, V. B. Shenoy, G. Eda, M. Chhowalla, *Nano Lett.* **2013**, *13*, 6222 – 6227; b) M. A. Lukowski, A. S. Daniel, F. Meng, A. Forticaux, L. Li, S. Jin, *J. Am. Chem. Soc.* **2013**, *135*, 10274; c) J. Xie, H. Zhang, S. Li, R. Wang, X. Sun, M. Zhou, J. Zhou, X. W. Lou, Y. Xie, *Adv. Mater.* **2013**, *25*, 5807; d) J. Xie, J. Zhang, S. Li, F. Grote, X. Zhang, H. Zhang, R. Wang, Y. Lei, B. Pan, Y. Xie, *J. Am. Chem. Soc.* **2013**, *135*, 17881; e) Y. Yu, S.-Y. Huang, Y. Li, S. N. Steinmann, W. Yang, L. Cao, *Nano Lett.* **2014**, *14*, 553; f) D. Voiry, H. Yamaguchi, J. W. Li, R. Silva, D. Alves, T. Fujita, M. W. Chen, T. Asefa, V. Shenoy, G. Eda, M. Chhowalla, *Nat. Mater.* **2013**, *12*, 850; g) T. Fujita, Y. Ito, Y. Tan, H. Yamaguchi, D. Hojo, A. Hirata, D. Voiry, M. Chhowalla, M. W. Chen, *Nanoscale* **2014**,*6*, 12458 – 12462.

[13] H.-J. Qiu, J. L. Kang, P. Liu, A. Hirata, T. Fujita, M. W. Chen, *J. Power Sources* **2014**, *247*, 896.

[14] a) Y. Ito, Y. Tanabe, H.-J. Qiu, K. Sugawara, S. Heguri, N. H. Tu, K. K. Huynh, T. Fujita, T. Takahashi, K. Tanigaki, M. Chen,

Angew. Chem. Int. Ed. **2014**, *53*, 4822 – 4826; *Angew. Chem.* **2014**, *126*, 4922 – 4926; b) Y. Ito, H.-J. Qiu, T. Fujita, Y. Tanabe, K. Tanigaki, M. Chen, *Adv. Mater.* **2014**, *26*, 4145 – 4150.

[15] S. Brunauer, P. H. Emmett, E. Teller, *J. Am. Chem. Soc.* **1938**, *60*, 309.

[16] E. P. Barrett, L. G. Joyner, P. H. Halenda, *J. Am. Chem. Soc.* **1951**, *73*, 373.

[17] a) T. Kondo, S. Casolo, T. Suzuki, T. Shikano, M. Sakurai, Y. Harada, M. Saito, M. Oshima, M. I. Trioni, G. F. Tantardini, J. Nakamura, *Phys. Rev. B* **2012**, *86*, 035436; b) Y. Ito, C. Christodoulou, M. V. Nardi, N. Koch, H. Sachdev, K. Muellen, *ACS Nano* **2014**, *8*, 3337 – 3346.

[18] X. Zhao, Q. Zhang, C.-M. Chen, B. Zhang, S. Reiche, A. Wang, T. Zhang, R. Schlögl, D. S. Su, *Nano Energy* **2012**, *1*, 624 – 630.

[19] W. Kiciński, M. Szala, M. Bystrzejewski, *Carbon* **2014**, *68*, 1.

[20] Y. W. Tan, P. Liu, L. Y. Chen, W. T. Cong, Y. Ito, J. H. Han, X. W. Guo, Z. Tang, T. Fujita, A. Hirata, M. W. Chen, *Adv. Mater.* **2014**, DOI: 10.1002/adma.201403808.

[21] N. H. Shon, T. Ando, *J. Phys. Soc. Jpn.* **1998**, *67*, 2421 – 2429.

[22] a) J. K. Nørskov, T. Bligaard, J. Rossmeisl, C. H. Christensen, *Nat. Chem.* **2009**, *1*, 37 – 46; J. K. Nørskov, T. Bligaard, A. Logadottir, J. R. Kitchin, J. G. Chen, S. Pandelov, U. Stimming, *J. Electrochem. Soc.* **2005**, *152*, J23 – J26; b) J. Greeley, T. F. Jaramillo, J. Bonde, I. Chorkendorff, J. K. Norskov, *Nat. Mater.* **2006**, *5*, 909 – 913.